

Gravitational Wave Emission from Close-in Strange Quark Planets Around Strange Stars with Magnetic Interactions

Xiao-Li Zhang,¹ Ze-Cheng Zou,² Yong-Feng Huang,^{2,3*} Hao-Xuan Gao,⁴ Pei Wang,^{5,6} Lang Cui,⁷ and Xiang Liu⁷

¹*Department of Physics, Nanjing University, Nanjing 210093, China*

²*School of Astronomy and Space Science, Nanjing University, Nanjing 210023, China*

³*Key Laboratory of Modern Astronomy and Astrophysics (Nanjing University), Ministry of Education, Nanjing 210023, China*

⁴*Purple Mountain Observatory, Chinese Academy of Sciences, Nanjing 210023, China*

⁵*National Astronomical Observatories, Chinese Academy of Sciences, Beijing 100101, China*

⁶*Institute for Frontiers in Astronomy and Astrophysics, Beijing Normal University, Beijing 102206, China*

⁷*Xinjiang Astronomical Observatory, Chinese Academy of Sciences, 150 Science 1-Street, Urumqi 830011, China*

Accepted XXX. Received YYY; in original form ZZZ

ABSTRACT

According to the strange quark matter hypothesis, strange planets may exist, which are planetary mass objects composed of almost equal numbers of up, down and strange quarks. A strange planet can revolve around its host strange star in a very close-in orbit. When it finally merges with the host, strong gravitational wave emissions will be generated. Here the gravitational waveforms are derived for the merging process, taking into account the effects of the strange star's magnetic field on the dynamics. Effects of the inclination angle are also considered. Templates of the gravitational waveforms are derived. It is found that the magnetic interactions significantly speed up the merging process. Coalescence events of such strange planetary systems occurring in our Galaxy as well as in local galaxies can be effectively detected by current and future gravitational experiments, which may hopefully provide a new method to test the strange quark matter hypothesis and probe the magnetic field of compact stars.

Key words: gravitational waves – exoplanets – stars: neutron – planet-star interactions – binaries: general – stars: magnetic fields

1 INTRODUCTION

The detection of the binary black hole merger event GW150914 by the LIGO–Virgo Collaboration (Abbott et al. 2016a) marks the beginning of gravitational-wave (GW) astronomy. The following years witnessed an incredibly increasing number of detected GW events from binary black hole mergers (Abbott et al. 2016b, 2017a,b,d, 2020a), binary neutron star mergers (Abbott et al. 2017c, 2020b), and even neutron star–black hole mergers (Abbott et al. 2020c, 2021). A larger range of astrophysics has become accessible through GWs, which provide new insights into the nature of the Universe. Especially, GWs are found to be able to help probe the interiors of compact stars thanks to the detection of GW170817 (for a review, see Guerra Chaves & Hinderer 2019).

Nevertheless, the exact composition and structure of compact stars are still elusive after huge efforts (for a recent review, see Menezes 2021). According to the strange quark matter (SQM) hypothesis (Farhi & Jaffe 1984; Witten 1984), nuclei consisting of baryons will undergo a phase transition and become a mixture composed of three quark flavors (up, down, and strange quarks) when they are subject to an extremely high pressure. Consequently, strange quark stars can stably exist and pulsars may actually be strange stars (Itoh 1970; Alcock et al. 1986; Haensel et al. 1986; Geng et al. 2021).

GW emissions from merging binary strange stars should be different from that of merging binary neutron stars (Limousin et al. 2005; Zhu & Rezzolla 2021), but the difference is somewhat subtle and difficult to be discerned by current GW experiments (Alford et al. 2019).

The self-bound nature of SQM means that strange quark nuggets would be stable. Consequently, SQM objects of planetary mass, i.e. strange planets, can also stably exist. Therefore, searching for strange planets would provide a direct test for the SQM hypothesis (Geng et al. 2015; Huang & Yu 2017; Kuerban et al. 2019, 2020). Various processes can lead to the formation of strange planets around compact stars (Xu 2006; Horvath 2012). A distinct feature of strange planets is that they can be very close to their hosts. A normal planet will be tidally disrupted if its orbit period (T) is less than ~ 6100 s, while a strange planet can still safely exist even for a much smaller period due to its high density. Such a period criterion can be used to distinguish strange planets from normal matter ones (Geng et al. 2015; Huang & Yu 2017; Kuerban et al. 2019, 2020; Wang et al. 2023), although searching for such small period pulsar planets through timing observations is still challenging (Perryman 2018).

A close-in strange planet–compact star system can emit very strong GWs, while a normal planet will be tidally disrupted far before the GW emission becomes significant. Geng et al. (2015) studied the GW emissions from close-in SQM planetary systems and argued that such GW signals can be used to probe SQM objects. It is found that a heavier strange quark planet will lead to a quicker merging

* E-mail: hyf@nju.edu.cn (Y-FH)

process associated with a higher GW amplitude (Geng et al. 2015). Kuerban et al. (2020) further investigated the GW emissions from ten candidates of close-in SQM planet systems in which the masses of the strange quark planets are different. They argued that the merger-induced GW emissions can be potentially detected by the advanced LIGO and Einstein Telescope (see Figure 4 of Kuerban et al. (2020)). It is worth noting that in these previous studies (Geng et al. 2015; Kuerban et al. 2019, 2020), researchers have mainly concentrated on the impact of planet mass on GW emissions. However, a compact star usually has a strong magnetic field, which will interact with the strange planet and change the dynamics of the system. Therefore, in this study, we will consider the effects of magnetic field and solve the problem numerically to obtain a set of GW templates for merging strange planet-compact star systems.

The structure of our paper is organized as follows. The magnetic field interactions and the GW emission process are modeled in Section 2. Our numerical results and the GW templates are presented in Section 3. Finally, Section 4 presents our conclusions and some brief discussion.

2 MODEL

2.1 Magnetic Interactions

For a rotating strange star, the radius of the light cylinder is mainly determined by its rotation speed, i.e.

$$r_c = \frac{c}{\Omega} = 6.7 \times 10^6 \left(\frac{\nu}{716 \text{ Hz}} \right)^{-1} \text{ cm}, \quad (1)$$

where c is the speed of light, Ω and ν are the angular rotation velocity and rotation frequency of the strange star, respectively (Lyne et al. 2022). The faster a compact star rotates, the smaller its light cylinder radius will be. Till now, the fastest rotating millisecond pulsar ever observed has a rotation frequency of $\nu = 716 \text{ Hz}$ (Hessels et al. 2006). Its light cylinder radius is as small as $6.7 \times 10^6 \text{ cm}$, but is still much larger than the typical radius of neutron stars and strange stars.

The strange planet will directly interact with the strange star's magnetosphere when its orbit is inside the light cylinder. Note that the tidal disruption radius of the strange planet is (Geng et al. 2015; Huang & Yu 2017)

$$r_{\text{td}} = 1.5 \times 10^6 \left(\frac{M}{1.4 M_\odot} \right)^{1/3} \left(\frac{\rho}{4 \times 10^{14} \text{ g cm}^{-3}} \right)^{-1/3} \text{ cm}, \quad (2)$$

where M is the mass of the strange star and $\rho \sim 4 \times 10^{14} \text{ g cm}^{-3}$ is the mean density of the strange planet. We see that r_{td} is only slightly larger than the radius of the strange star, which means the strange planet can maintain its integrity even when it is very close to the strange star surface. Combining Equations (1) and (2), we can safely regard the strange planet as an intact sphere when it interacts with the magnetosphere of the strange star inside the light cylinder.

When orbiting around the strange star inside the magnetosphere, the strange planet will travel across the magnetic field lines which gives birth to a strong electric field. In the magnetosphere that is full of free electrons, this will lead to strong electric currents and correspondingly, a strong electromotive force exerted on the strange planet itself. According to the popular unipolar induction direct current (DC) model (Piddington & Drake 1968; Goldreich & Lynden-Bell 1969), the kinetic energy of the planetary system will be dissipated through Ohmic dissipation, which is determined by the total resistance of the circuit. In our framework, the surface of a bare strange planet is covered by a layer of free electrons (Alcock et al. 1986). Therefore, the strange planet can be regarded as a superconductor.

Lai (2012) proved that the Ohmic dissipation will not grow up to infinity even when the total resistance is extremely small. Instead, it has an upper limit because a large current will twist the magnetic flux tubes and destroy the circuit. As a result, the energy loss rate of the system due to the magnetic interaction is (Lai 2012)

$$\dot{E}_{\text{mag}} = -\zeta_\phi (\omega - \Omega) \frac{\mu^2 r^2}{2a^5}, \quad (3)$$

where $0 < \zeta_\phi < 1$ is a coefficient describing the twist of the magnetic flux tube, μ is the magnetic moment of the strange star, ω , r , and a are the strange planet's orbital angular velocity, radius, and orbit radius, respectively. According to the refined direct circuit model proposed by Lai (2012), the maximum energy dissipation, i.e. the smallest total resistance limit, occurs when $\zeta_\phi = 1$.

2.2 Dynamics and GW Emissions

In addition to the energy dissipation from magnetic interactions, the system is also subjected to energy dissipation caused by GW emissions. To analyze the GW effects on the dynamics, we assume a quasi-circular orbit for the system for simplicity. Denoting the strange planet's mass as m , energy loss rate due to GW emissions can be expressed as (Landau & Lifshitz 1975; Creighton & Anderson 2011; Postnov & Yungelson 2014)

$$\dot{E}_{\text{GW}} = -\frac{32G^4 M^2 m^2 (M+m)}{5c^5 a^5}, \quad (4)$$

where G is the gravitational constant.

The dynamical evolution of the system can be solved numerically by combining Equations (3) and (4). After a small time interval δt , the loss of the orbital energy is

$$\delta \left(-\frac{GMm}{2a} \right) = (\dot{E}_{\text{mag}} + \dot{E}_{\text{GW}}) \delta t. \quad (5)$$

The orbit will shrink as time goes on. The orbital phase at time t can then be calculated as

$$\varphi = \int_0^t \omega(t) dt = \int_0^t \frac{2\pi}{T(t)} dt, \quad (6)$$

where T is the orbital period.

After solving the dynamics, we can easily calculate the waveform of the emitted GWs. For an observer at a viewing angle of ι (the inclination angle with respect to the normal of the orbital plane), the waveform can be expressed as (Creighton & Anderson 2011)

$$\begin{aligned} h_+ &= -\frac{4Gu^2 \omega^2}{c^4 d} \frac{1 + \cos^2 \iota}{2} \cos 2\varphi, \\ h_\times &= -\frac{4Gu^2 \omega^2}{c^4 d} \cos \iota \sin 2\varphi, \end{aligned} \quad (7)$$

where h_+ and h_\times denote the two polarizations of GWs, $u = Mm/(M+m)$ is the reduced mass of the strange planet-strange star system, and d is the luminosity distance.

3 RESULTS

Using the equations described above, we have solved the merging process of strange star-strange planet systems and computed GW emissions numerically. In our calculations, the mass of the strange star is fixed as $M = 1.4 M_\odot$, while three masses are taken for the strange planet, i.e. $m = 10^{-3}, 10^{-4},$ and $10^{-5} M_\odot$. The distance of the planetary system is taken as 10 kpc. The initial separation between

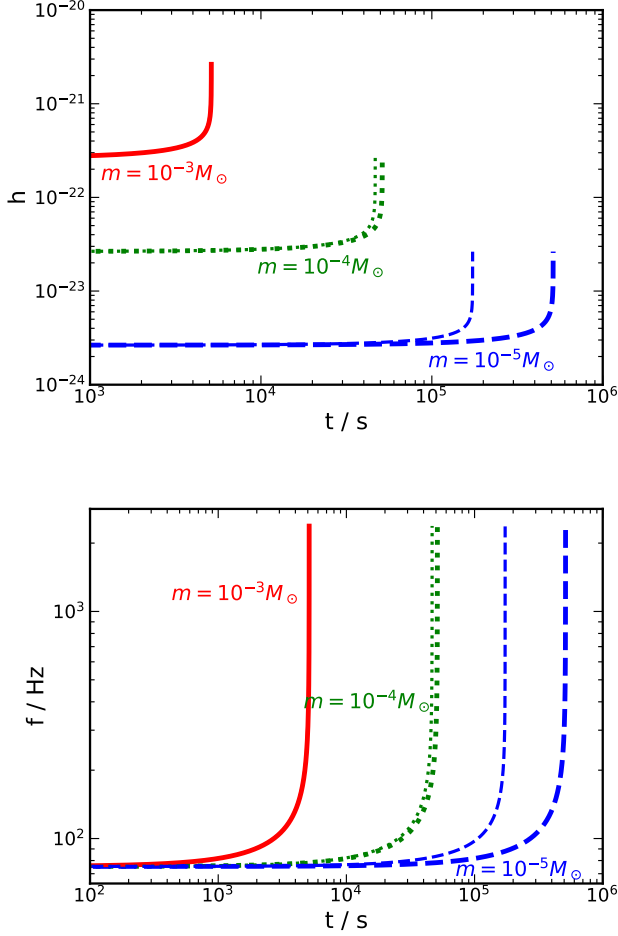


Figure 1. Evolution of the GWs emitted from merging strange star-strange planet systems which are assumed to be face-on. The upper panel shows the evolution of the effective strain amplitude (h) and the lower panel shows the evolution of the frequency (f). In each panel, the solid, dotted and dashed curves correspond to the strange planet mass of $m = 10^{-3}$, 10^{-4} , and $10^{-5} M_{\odot}$, respectively. For the thick curves, the magnetic moment of the strange star is taken as zero ($\mu = 0$), while for the thin curves, the magnetic moment is assumed to be $\mu = 10^{33} \text{ G cm}^3$ (corresponding to a surface magnetic field of $\sim 10^{15} \text{ G}$ for the strange star). Note that in the case of $m = 10^{-3} M_{\odot}$, the effect of the magnetic field is almost negligible so that the thick curve and the thin curve are essentially overlapped.

the strange star and the planet is assumed to be $1.5 \times 10^7 \text{ cm}$. To assess the effects of the magnetic field, we take the magnetic moment as $\mu = 10^{33} \text{ G cm}^3$, which corresponds to a strongly magnetized magnetar with a surface field of $B \sim 10^{15} \text{ G}$ (Duncan & Thompson 1992; Woods & Thompson 2006; Kaspi 2010; Mereghetti et al. 2015; Turolla et al. 2015; Kaspi & Beloborodov 2017). The results are compared with those of the $\mu = 0$ ($B = 0$) cases.

The effective strain amplitude is $h = \sqrt{h_+^2 + h_{\times}^2}$, which can be calculated by using Equation (7). The upper panel of Figure 1 illustrates the evolution of h during the inspiral process for face-on systems ($\iota = 0$). We see that for a more massive strange planet, the system will merge more quickly and the GW emission is correspondingly stronger. The magnetic interaction accelerates the merging process, especially for the light strange planet cases. The evolution of the GW frequency ($f = 2/T$) is plotted in the lower panel of Figure 1. The

frequency is mainly $\sim 100 - 1000 \text{ Hz}$, which falls in the frequency range of most ground-based GW detectors. Again, we see that the existence of the magnetic field speeds up the merging process.

Figure 2 shows the evolution of the “plus” polarization GW waveforms for merging strange star-strange planet systems. The effect of magnetic interactions is not considered here ($\mu = 0$), and the systems are assumed to be face-on ($\iota = 0$). In fact, the “envelopes” of these waveforms are just those strain amplitude curves shown in Figure 1. Note that both the X and Y axes are in linear scale rather than in logarithmic scale, which can help illustrate the evolution of the GW waveforms more directly and also facilitates a clear comparison with the following cases including magnetic interactions. From Figure 2, we see that the coalescence timescale is inversely correlated with the planet mass (m). For example, when $m = 10^{-3} M_{\odot}$, the coalescence timescale is $\sim 5.12 \times 10^3 \text{ s}$ (the top panel). It increases to $\sim 5.13 \times 10^4 \text{ s}$ for $m = 10^{-4} M_{\odot}$ (the middle panel), and increases to $\sim 5.13 \times 10^5 \text{ s}$ for $m = 10^{-5} M_{\odot}$ (the bottom panel). At the same time, the strain amplitude is proportional to m . These behaviors are consistent with Equation (7). The effects of inclination angle on the GW waveforms are illustrated in Figure 3. Three different inclinations, i.e. $\iota = 0$ (face-on), $\iota = \pi/4$, and $\iota = \pi/2$ (edge-on), are considered here as typical examples. The effect of magnetic interactions is also not included here ($\mu = 0$). The insets show a zoom in of the GW waveform at four typical moments, with the time marked on the horizontal axis correspondingly. We see that the GW amplitude becomes smaller as ι increases, and a face-on observer would see the strongest GW emissions.

Figure 4 shows the evolution of the h_+ component in cases of strong magnetic interactions. We take a magnetic moment of $\mu = 10^{33} \text{ G cm}^3$ for the strange star. Comparing Figure 4 with Figure 2, we find that the magnetic field interaction significantly shortens the coalescence timescale for the light strange planet cases. For example, when $m = 10^{-5} M_{\odot}$, the coalescence timescale is $\sim 5.13 \times 10^5 \text{ s}$ in the $\mu = 0$ case (see the bottom panel of Figure 2), but it is $\sim 1.73 \times 10^5 \text{ s}$ in the $\mu = 10^{33} \text{ G cm}^3$ case (see the bottom panel of Figure 4). The timescale is reduced by a factor of about two-thirds due to the magnetic interaction. On the other hand, when the mass of the strange planet is larger, the effect becomes less significant. For the planet mass of $m = 10^{-3} M_{\odot}$, the coalescence timescale is $\sim 5.12 \times 10^3 \text{ s}$ in the $\mu = 0$ case (see the top panel of Figure 2), and it is $\sim 5.10 \times 10^3 \text{ s}$ in the $\mu = 10^{33} \text{ G cm}^3$ case (see the top panel of Figure 4). These two timescales differ only slightly. The effect of magnetic field can be easily understood by combining Equations (3) and (4): the energy dissipation rate due to GW emission scales with the planet mass as $\dot{E}_{\text{GW}} \propto m^2$, while the magnetic interaction scales as $\dot{E}_{\text{mag}} \propto r^2 \propto m^{2/3}$. Therefore, the more massive the strange planet is, the less significant the magnetic interaction will be as compared with the GW dissipation. Figure 5 presents a direct comparison of the GW waveforms for the cases with/without magnetic interactions. One can see that at early stages, the waveforms are almost identical for the two cases. As time goes on, the frequency becomes slight different so that the phase shift becomes obvious. At the final chirp stage, the waveform is essentially quite different in the two cases. It hints that the GW observations may potentially provide some useful clues for measuring the magnetic field of such compact stars.

To successfully observe a GW signal, its strain spectral amplitude should be higher than the sensitivity curve of GW detectors. Ground-based detectors mainly operates in the frequency domain. We thus need to analyze the GW signals via the Fourier transform method. Adopting the stationary phase approximation, the Fourier transform of the h_+ component of GW emissions can be expressed as (Moore

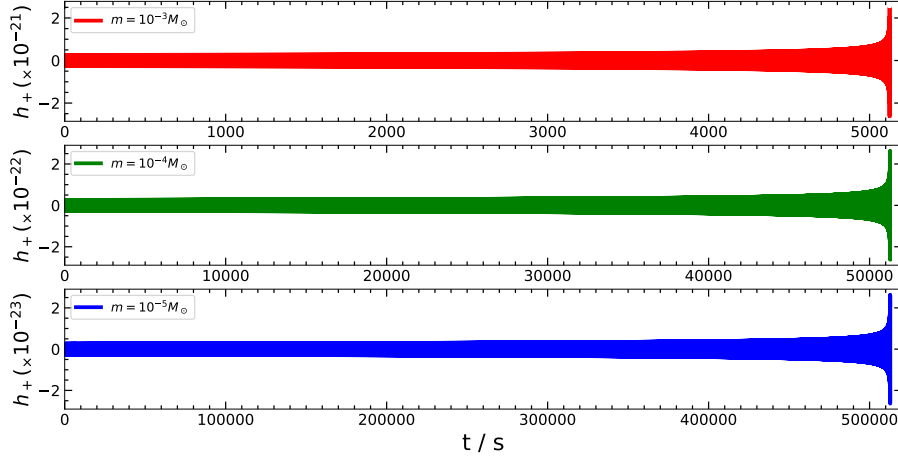


Figure 2. Evolution of the GW profile (the h_+ component) for merging strange star-strange planet systems. The systems are assumed to be face-on and no magnetic interactions are considered ($\mu = 0$). Three different masses are assumed for the strange planet, i.e. $m = 10^{-3}$, 10^{-4} , and $10^{-5} M_{\odot}$, respectively.

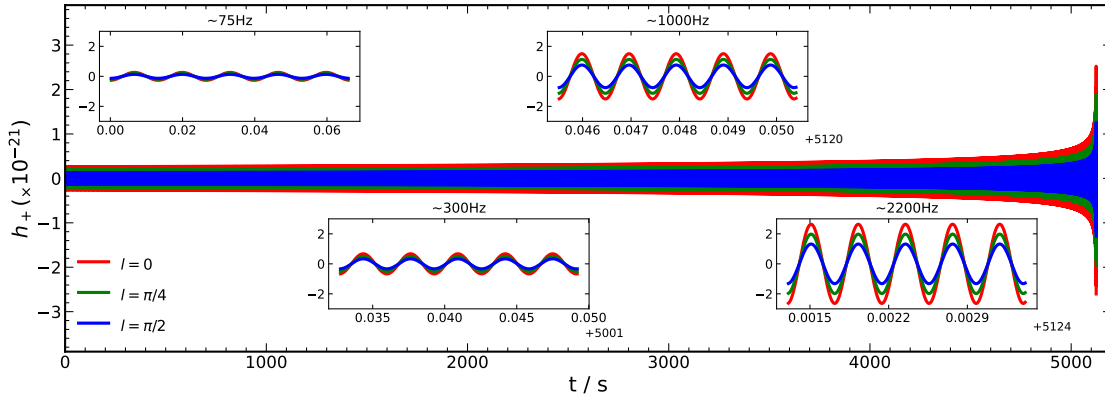


Figure 3. Effects of the inclination angle on the GW profile (the h_+ component). Three different inclination angles, i.e. $\iota = 0$ (face-on), $\iota = \pi/4$, and $\iota = \pi/2$ (edge-on), are shown in the plot. Here we take the magnetic moment of the strange star as $\mu = 0$. The mass of the strange planet is $m = 10^{-3} M_{\odot}$. The insets show a zoom in of the GW profile at four moments, which correspond to a frequency of ~ 75 , 300, 1000, and 2200 Hz, respectively.

et al. 2015)

$$\tilde{h}_+(f) \approx \frac{h_0}{\sqrt{2}} \int_{-\infty}^{+\infty} \left[\exp(2\pi i f t^2) + \exp(-2\pi i f t^2) \right] dt \approx \frac{h_0}{\sqrt{2f}}, \quad (8)$$

where

$$h_0 = \frac{h_+}{\sqrt{2} \cos 2\varphi}. \quad (9)$$

The \tilde{h}_\times polarization component can also be calculated similarly. The overall average of the Fourier transform function is then

$$\tilde{h}(f) = \sqrt{\langle \tilde{h}_+^2(f) \rangle + \langle \tilde{h}_\times^2(f) \rangle}. \quad (10)$$

Using this expression, the GW strain spectral amplitude (square root of the GW power spectral density; Moore et al. 2015; Zou et al. 2020; Zou & Huang 2022) can finally be derived as

$$h_f = 2f^{1/2} |\tilde{h}(f)|. \quad (11)$$

Figure 6 plots the strain spectral amplitude of various face-on strange star-strange planet systems. Generally, the amplitude is higher when the planet mass is larger. In the $\mu = 0$ cases, the $\lg h_f - \lg f$ plots are essentially straight lines with a universal slope of $-2/3$, which is consistent with the analytical expectations (Moore et al. 2015). When the magnetic interactions take effect, the $\lg h_f - \lg f$ plots deviate from the straight lines obviously. The deviation is more significant when the planet mass is smaller. It further clearly shows that the magnetic field of the compact star leads to different behavior of the GW emission, which could potentially be used to measure the magnetic field strength of compact stars.

The sensitivity curves of the advanced Laser Interferometer Gravitational-wave Observatory¹ (ad-LIGO, O3 stage; Harry & LIGO Scientific Collaboration 2010), the future Einstein Telescope

¹ <https://dcc-lho.ligo.org/LIGO-T2000012/public>

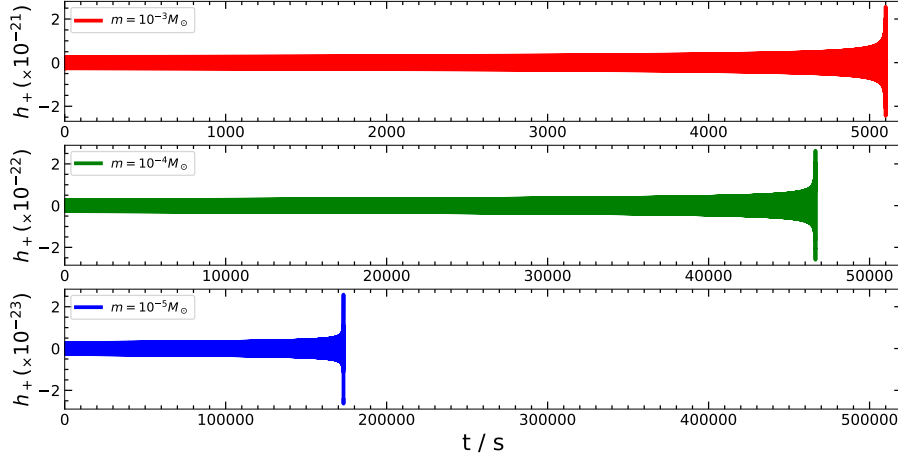


Figure 4. Evolution of the GW profile (the h_+ component) for merging strange star-strange planet systems. The systems are assumed to be face-on. The magnetic moment of the strange star is taken as $\mu = 10^{33} \text{ G cm}^3$. Three different masses are assumed for the strange planet, i.e. $m = 10^{-3}, 10^{-4}$, and $10^{-5} M_\odot$, respectively.

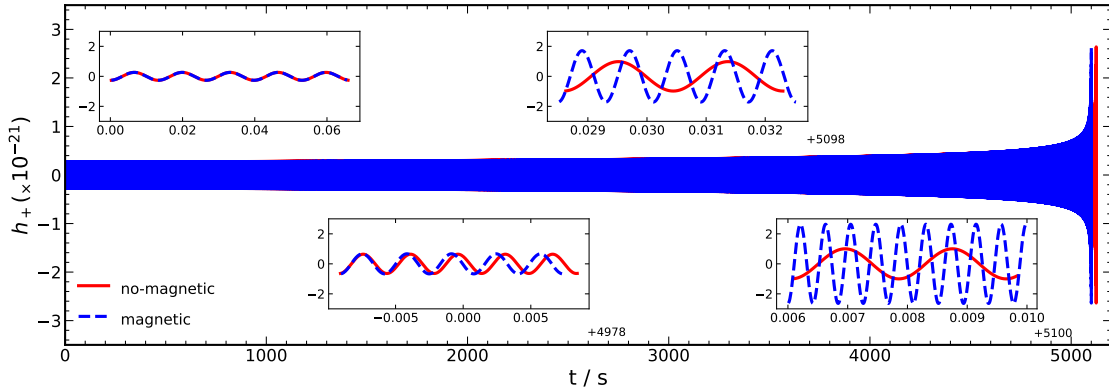


Figure 5. A direct comparison of the GW waveforms for the cases with/without magnetic interactions. The systems are assumed to be face-on, and the mass of the strange planet is $m = 10^{-3} M_\odot$. The solid curve corresponds to the $\mu = 0$ case and the dashed curve corresponds to a magnetic moment of $\mu = 10^{33} \text{ G cm}^3$ for the strange star. The insets show a zoom in of the GW profile at four exemplar moments.

designed in 2011² (ET-D; Hild et al. 2008, 2011; Maggiore et al. 2020) and the updated future Einstein Telescope designed in 2021 with the length of arms taken as 20 km³ (ET-20km arm; Branchesi et al. 2023) are also plotted in Figure 6 for a direct comparison. We see that the amplitudes are generally much higher than the sensitivity curves, thus such a kind of GW signals could potentially be detected by current and future GW experiments. In fact, GW emissions from merging strange star-strange planets in local galaxies up to a distance of several Mpc could also be detectable (Geng et al. 2015). Signals from such events with an extreme mass ratio ($> 10^3 - 10^4$) are suggested to be paid special attention in current and future GW observations.

4 CONCLUSIONS AND DISCUSSION

In this study, the inspiral and merging process of a strange planet with respect to its host strange star is investigated, aiming to provide detailed GW waveform information and GW templates for detecting such events by using current and future GW experiments. The effect of the inclination angle is considered and the magnetic interaction is included. It is found that a strong magnetic field of the strange star can markedly speed up the inspiral process, leading to a much shorter coalescence timescale. The effect of magnetic interactions is more significant for the less massive strange planet cases. By comparing the strain spectral amplitude of GWs with the sensitivity curves of ad-LIGO and ET, it is shown that the merging events occurring in our Galaxy can be detected by these GW experiments. The effects of magnetic interactions can be discerned from GW observations, hopefully providing a new method to measure the magnetic field of compact stars.

It is worth mentioning that primordial black holes (PBH) can

² <https://www.et-gw.eu/index.php/etsensitivities>

³ <https://apps.et-gw.eu/tds/ql/?c=16492>

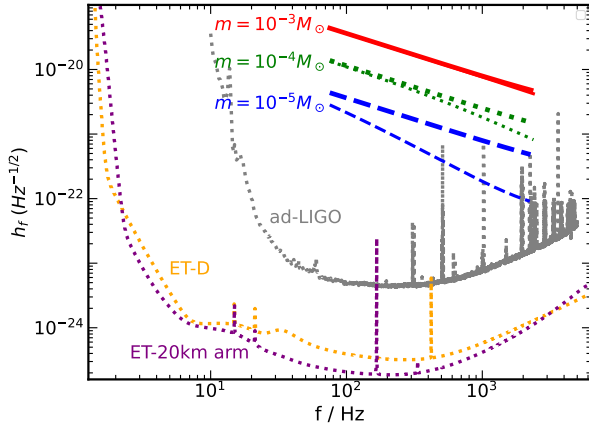


Figure 6. Strain spectral amplitude of GWs from various strange star-strange planet systems, plotted versus frequency. The planetary systems are assumed to be face-on, and the distance is 10 kpc. The mass of the strange planet is taken as $m = 10^{-3}$, 10^{-4} and $10^{-5} M_{\odot}$, respectively. For the thick curves, the magnetic moment of the strange star is taken as zero ($\mu = 0$), while for the thin curves, the magnetic moment is assumed to be $\mu = 10^{33} \text{ G cm}^3$. The sensitivity curves of the ad-LIGO O3, ET-D (Einstein Telescope designed in 2011), and ET-20km arm (the updated Einstein Telescope with 20 km arms designed in 2021) are also plotted for a direct comparison.

be captured by compact stars and form close-in planetary systems (Génolini et al. 2020). In these systems, when the planetary-mass PBH finally merges with the compact star, strong GW emissions will also be generated, whose characteristics should be very similar to the cases studied here. Still we can hopefully distinguish the strange star-strange planet mergers from the compact star-PBH mergers by considering their different behaviors in the ring down stage. After a PBH comes into the surface of its host, it will keep tunneling inside the compact star and inspiral towards the center. In this process, a strong ring down signal will be generated in the GW emission, which can be detected by ad-LIGO at a high confidence level (Zou & Huang 2022). Additionally, a compact star-PBH merger will end up with a strong electromagnetic outburst, since the compact star will finally be swallowed by the PBH. By contrast, a strange planet will finally collide and coalesce with the host strange star, producing relative shorter and much weaker ring down signals.

Close-in planets are usually found to be tidally locked (Perryman 2018). However, in our study, such a tidal effect has not been considered. This is acceptable because the tidal deformability of strange planets are generally very small (Wang et al. 2021). Anyway, at the final stage of the merging process, tidal deformability may still take effect on the GW waveform when the strange planet approaches the surface of the strange star. This effect may need to be further addressed in future studies.

Targeted filter-matched searches in archival GW data have already yielded many interesting results (e.g., Nitz 2018; Wang & Nitz 2021, 2024). With the GW templates available for merging strange planetary systems, an in-depth search for GW signals corresponding to these extreme mass ratio merging events in currently available GW data as well as in future GW experiments is solicited, which will help test the SQM hypothesis and probe the nature of dense nuclear matter.

ACKNOWLEDGMENTS

Z.-C Z. gratefully acknowledges An-Dong Chen for enlightening discussion on exoplanet detection. This study was supported by the National Natural Science Foundation of China (Grant Nos. 12233002, 11988101, U2031117), by the National SKA Program of China Nos. 2020SKA0120300, 2020SKA0120200 and No. 2022SKA0120102, by the National Key R&D Program of China (2021YFA0718500, 2023YFE0102300), by the CAS “Light of West China” Program (No. 2021-XBQNXXZ-005), and by Xinjiang Tianshan Talent Program. YFH also acknowledges the support from the Xinjiang Tianshan Program.

DATA AVAILABILITY

No new data were generated or analysed in support of this research.

REFERENCES

- Abbott B. P., et al., 2016a, *Phys. Rev. Lett.*, **116**, 061102
 Abbott B. P., et al., 2016b, *Phys. Rev. Lett.*, **116**, 241103
 Abbott B. P., et al., 2017a, *Phys. Rev. Lett.*, **118**, 221101
 Abbott B. P., et al., 2017b, *Phys. Rev. Lett.*, **119**, 141101
 Abbott B. P., et al., 2017c, *Phys. Rev. Lett.*, **119**, 161101
 Abbott B. P., et al., 2017d, *ApJ*, **851**, L35
 Abbott R., et al., 2020a, *Phys. Rev. Lett.*, **125**, 101102
 Abbott B. P., et al., 2020b, *ApJ*, **892**, L3
 Abbott R., et al., 2020c, *ApJ*, **896**, L44
 Abbott R., et al., 2021, *ApJ*, **915**, L5
 Alcock C., Farhi E., Olinto A., 1986, *ApJ*, **310**, 261
 Alford M. G., Han S., Schwenzer K., 2019, *Journal of Physics G Nuclear Physics*, **46**, 114001
 Branchesi M., et al., 2023, *J. Cosmology Astropart. Phys.*, **2023**, 068
 Creighton J., Anderson W., 2011, *Gravitational-Wave Physics and Astronomy: An Introduction to Theory, Experiment and Data Analysis*.
 Duncan R. C., Thompson C., 1992, *ApJ*, **392**, L9
 Farhi E., Jaffe R. L., 1984, *Phys. Rev. D*, **30**, 2379
 Geng J. J., Huang Y. F., Lu T., 2015, *ApJ*, **804**, 21
 Geng J., Li B., Huang Y., 2021, *The Innovation*, **2**, 100152
 Génolini Y., Serpico P. D., Tinyakov P., 2020, *Phys. Rev. D*, **102**, 083004
 Goldreich P., Lynden-Bell D., 1969, *ApJ*, **156**, 59
 Guerra Chaves A., Hinderer T., 2019, *Journal of Physics G Nuclear Physics*, **46**, 123002
 Haensel P., Zdunik J. L., Schaefer R., 1986, *A&A*, **160**, 121
 Harry G. M., LIGO Scientific Collaboration 2010, *Classical and Quantum Gravity*, **27**, 084006
 Hessels J. W. T., Ransom S. M., Stairs I. H., Freire P. C. C., Kaspi V. M., Camilo F., 2006, *Science*, **311**, 1901
 Hild S., Chelkowski S., Freise A., 2008, *arXiv e-prints*, p. arXiv:0810.0604
 Hild S., et al., 2011, *Classical and Quantum Gravity*, **28**, 094013
 Horvath J. E., 2012, *Research in Astronomy and Astrophysics*, **12**, 813
 Huang Y. F., Yu Y. B., 2017, *ApJ*, **848**, 115
 Itoh N., 1970, *Progress of Theoretical Physics*, **44**, 291
 Kaspi V. M., 2010, *Proceedings of the National Academy of Science*, **107**, 7147
 Kaspi V. M., Beloborodov A. M., 2017, *ARA&A*, **55**, 261
 Kuerban A., Geng J.-J., Huang Y.-F., 2019, in *Xiamen-CUSTIPEN Workshop on the Equation of State of Dense Neutron-Rich Matter in the Era of Gravitational Wave Astronomy*. p. 020027, doi:10.1063/1.5117817
 Kuerban A., Geng J.-J., Huang Y.-F., Zong H.-S., Gong H., 2020, *ApJ*, **890**, 41
 Lai D., 2012, *ApJ*, **757**, L3
 Landau L. D., Lifshitz E. M., 1975, *The classical theory of fields*
 Limousin F., Gondek-Rosińska D., Gourgoulhon E., 2005, *Phys. Rev. D*, **71**, 064012

- Lyne A., Graham-Smith F., Stappers B., 2022, *Pulsar Astronomy*, 5 edn. Cambridge Astrophysics, Cambridge University Press
- Maggiore M., et al., 2020, *J. Cosmology Astropart. Phys.*, 2020, 050
- Menezes D. P., 2021, *Universe*, 7, 267
- Mereghetti S., Pons J. A., Melatos A., 2015, *Space Sci. Rev.*, 191, 315
- Moore C. J., Cole R. H., Berry C. P. L., 2015, *Classical and Quantum Gravity*, 32, 015014
- Nitz A. H., 2018, *Classical and Quantum Gravity*, 35, 035016
- Perryman M., 2018, *The Exoplanet Handbook*. Cambridge university press
- Piddington J. H., Drake J. F., 1968, *Nature*, 217, 935
- Postnov K. A., Yungelson L. R., 2014, *Living Reviews in Relativity*, 17, 3
- Turolla R., Zane S., Watts A. L., 2015, *Reports on Progress in Physics*, 78, 116901
- Wang Y.-F., Nitz A. H., 2021, *ApJ*, 912, 53
- Wang Y.-F., Nitz A. H., 2024, *MNRAS*, p. stae091
- Wang X., Kuerban A., Geng J.-J., Xu F., Zhang X.-L., Zuo B.-J., Yuan W.-L., Huang Y.-F., 2021, *Phys. Rev. D*, 104, 123028
- Wang X., Huang Y.-F., Li B., 2023, in *The Sixteenth Marcel Grossmann Meeting. On Recent Developments in Theoretical and Experimental General Relativity*. pp 3118–3123, doi:10.1142/9789811269776_0254
- Witten E., 1984, *Phys. Rev. D*, 30, 272
- Woods P. M., Thompson C., 2006, in , Vol. 39, *Compact stellar X-ray sources*. pp 547–586, doi:10.48550/arXiv.astro-ph/0406133
- Xu R. X., 2006, *Astroparticle Physics*, 25, 212
- Zhu Z., Rezzolla L., 2021, *Phys. Rev. D*, 104, 083004
- Zou Z.-C., Huang Y.-F., 2022, *ApJ*, 928, L13
- Zou Z.-C., Zhou X.-L., Huang Y.-F., 2020, *Research in Astronomy and Astrophysics*, 20, 137

This paper has been typeset from a $\text{\TeX}/\text{\LaTeX}$ file prepared by the author.